Title:

Migration alters oscillatory dynamics and promotes survival in connected bacterial populations

Short title:

Synchrony and survival of connected populations

Authors:

Shreyas Gokhale*,[1], Arolyn Conwill*,[1], Tanvi Ranjan[2] and Jeff Gore[1,†]

[1] Physics of Living Systems, Department of Physics, Massachusetts Institute of Technology, Cambridge, MA 02139.

[2] John A. Paulson School of Engineering and Applied Sciences, Harvard University, Cambridge, MA 02138.

[†] To whom correspondence should be addressed. Email: gore@mit.edu

* These authors contributed equally to this work.

Classification:

Major category: Biological sciences

Minor category: Ecology / Population Biology

Abstract:

Migration influences population dynamics on networks and is therefore a key factor in diverse scenarios ranging from the extinction of rare species to the spread and control of epidemics. While isolated populations in a network are vulnerable to extinction due to demographic stochasticity or challenging environmental conditions, migration can stabilize such endangered populations via the influx of individuals from neighboring nodes (or patches). On the other hand, a large migratory flux can synchronize the population dynamics in connected patches, which enhances the risk of global extinction in harsh conditions. Here, we investigate this trade-off between local rescue and global extinction experimentally using two antibiotic resistant strains of *E. coli* that exhibit oscillatory population dynamics when co-cultured. We observe that high migration rates lead to in-phase synchronization of oscillations whereas intermediate migration

rates perturb the oscillations and change their period, highlighting that migration has a profound qualitative impact on population dynamics. Simulations using a mechanistic model of antibiotic deactivation by resistant bacteria are in agreement with our experimental findings. These simulations further predict that connected populations subjected to higher, more challenging antibiotic concentrations have the highest probability of survival at intermediate migration rates. Consistent with this prediction, our experiments reveal that moderate levels of migration help populations survive longer in this challenging environment. Our results clarify how migration between two patches can alter population dynamics and influence survival, and our study may help elucidate the impact of migration on much larger networks such as those studied in conservation biology and epidemiology.

Significance Statement:

Migration patterns dictate the dynamics of spatially extended populations in various contexts such as epidemic propagation, species conservation, and ecological invasion. Low migration rates might counter extinction by allowing for colonization of unoccupied habitats whereas high rates might promote it via synchronization and collapse of coupled populations. Here, we explore this tradeoff experimentally using two oscillating bacterial populations connected by migration. We show that migration can not only synchronize, but also alter oscillations, leading to qualitatively distinct behaviors not observed in isolated populations. Further, these altered oscillations can enhance the ability of populations to survive in challenging environments. Our study facilitates a deeper understanding synchronization and survival in the larger population networks relevant to conservation biology and epidemiology.

Introduction:

Spatially extended populations are often distributed heterogeneously in space, in the form of a network of densely populated regions, or patches, connected to each other by migration of individuals (1). From human settlements connected by transportation routes (2) to the distribution of species over distinct habitat patches (3), population networks are pervasive in a variety of social and ecological settings. The population dynamics on these networks are shaped by migration patterns (4), which can have a significant impact on population stability (5–7). In the absence of migration, the population dynamics in different patches unfold independently of

each other. Such disconnected networks, or fragmented habitats, are generally considered to be undesirable, because isolated populations are susceptible to extinction due to demographic stochasticity or environmental fluctuations (8). In the presence of migration, these endangered populations can be stabilized by migrants from neighboring populations (9). Furthermore, even if a local population becomes extinct, it can be re-colonized by individuals from nearby patches (8, 10). The idea that migration prevents populations from collapsing has led to the construction of 'conservation corridors' that prevent local extinctions by facilitating movement between previously unconnected habitats (11). While such local rescue effects are vital from the point of view of species conservation, excessive migration can lead to in-phase synchronization of population dynamics in connected habitat patches (12).

Under harsh environmental conditions, such synchronization can in turn enhance the risk of global extinction during periods of collective decrease in population size (13), since patches effectively merge into one large population in the limit of strong coupling (14). More concretely, these observations illustrate the tradeoff associated with the impact of migration on deterministic versus stochastic aspects of population dynamics. Because large migration rates can increase the overall population size on sparsely populated patches, migration can counteract stochastic extinction in a local population. However, deterministic oscillations in population dynamics, which may arise naturally due to predator-prey (15) or host-parasite (16) interactions, can become synchronized due to migration. This synchronization may cause the population size to decrease simultaneously across the entire network, enhancing the risk of collective stochastic extinction in all connected patches (13).

While it is natural to think of migration in the context of birds or terrestrial mammals, it plays an important role in shaping the spatial population dynamics of microbes and even plants. For instance, plant populations can be coupled over long distances via seed dispersal (6, 17). Ocean microbes colonize organic particulate matter called marine snow (18), which plays a crucial role in the global carbon cycle (19). Local migration between neighboring particles not only allows these microbial communities to span enormous spatial regions, but also determines their composition and spatial structure. Pathogenic microbes take advantage of human transportation networks, which facilitate movement of infected individuals between cities and result in the

spread of epidemics (20). Interestingly, migration is known to synchronize epidemic outbreaks in distinct locations over long timescales for a variety of infectious diseases (21–23). Although synchronization is often undesirable from a conservation standpoint, it can be advantageous in the context of epidemics, since it facilitates coordinated vaccination campaigns (24, 25). These examples demonstrate that understanding the impact of migration on the population dynamics of spatially extended ecosystems may have implications not only for conservation, but also for carbon fixation and epidemic eradication.

Despite the importance of migration patterns in ecology and epidemiology, there is little in-depth understanding of how migration impacts population dynamics, particularly when the migration rate is between the limits of no coupling (independent populations) and high coupling (synchronized populations) (Fig. 1). Experiments in field ecology are challenging due to long time scales, insufficient statistics, weather fluctuations, and natural as well as anthropogenic disturbances. The collection of demographic or epidemiological data on humans is also hindered by similar impediments as well as the inability to perform controlled manipulations. While theoretical (13, 26) and computational (27–30) work has led to a number of predictions regarding synchronization and extinction, directly verifying them in experiments has proven to be difficult, owing largely to the aforementioned complications associated with typical population networks.

Here, we develop a simple bacterial model system composed of two connected oscillating populations to elucidate the impact of migration on population dynamics (Fig. 1A). Our system forgoes the complexity of natural population networks, but allows precise control over migration rates and environmental conditions, enabling a level of quantitative detail that is not typically attainable in the field. We also use a mathematical model of our experimental populations to further investigate the effects of migration between patches. We first quantify the onset of in-phase synchronization in benign environmental conditions, in which individual populations exhibit stable oscillations over the duration of the experiment (Fig. 1B). More importantly, we show that en route to synchronization, the system goes through a series of qualitatively distinct oscillatory dynamics that are not observed in the absence of migration. We further show that these new dynamics enable populations to endure longer in harsh environments, as evidenced by the increase in survival times for moderate levels of migration. We emphasize that intermediate

125 migration rates can lead to different ecological outcomes, even though the migration rate is
126 below the level necessary for the onset of synchronization (Fig. 1B). In a broader context, our
127 results on two connected bacterial populations can be viewed as the first step in a bottom up
128 approach aimed at understanding the role of migration in the population dynamics of more
129 complex networks.
130
131 **Results:**
132 In order to quantify effects such as synchronization in an experimental model system, we use a
133 bacterial cross-protection mutualism that exhibits robust oscillatory population dynamics (31).
134 The system is comprised of two strains of *Escherichia coli* that protect each other from
135 antibiotics in the environment by producing resistance enzymes. One strain (AmpR) is resistant
136 to the antibiotic ampicillin, and the other strain (ChlR) is resistant to the antibiotic
137 chloramphenicol (Fig. 2A). Previous work has already demonstrated that a co-culture of AmpR
138 and ChlR exhibits robust limit cycle oscillations as a function of time over a broad range of
139 antibiotic concentrations, when subjected to serial daily dilutions into fresh media and antibiotics
140 (31).
141
142 In the serial daily dilution scheme employed in our experiments (Fig. 2B), we propagated co-
143 cultures of the AmpR and ChlR strains in ~24 hour growth-dilution cycles in 96-well plates
144 under well-mixed conditions in the presence of LB media, ampicillin, and chloramphenicol. At
145 the end of each growth cycle, we measured the total population density using spectrophotometry
146 and the relative proportion of AmpR and ChlR cells using flow cytometry (See Materials and
147 Methods). Next, we diluted the co-cultures by a factor of 100 into fresh media containing
148 antibiotics, and subjected them to another growth cycle for ~24 hours. Upon repeating these
149 daily growth-dilution cycles for 15 days, we observed that the population density of AmpR
150 (purple) as well as ChlR (green) cells oscillates with a period of 3 days (Fig. 2C, left panel). We
151 note that the ratio of AmpR cells to ChlR cells constitutes an appropriate characterization of the
152 state of the population because it also exhibits period-3 oscillations, with the oscillation
153 amplitude spanning four orders of magnitude (Fig. 2C, right panel).
154

In order to examine the effects of migration, we studied pairs of co-cultures and coupled them via transfer of cells between the two patches of each pair. Fig. 3A depicts the growth-migration-dilution scheme employed in our experiments. The scheme is similar to the growth-dilution scheme discussed earlier (Fig. 2B), with two important additions. First, we consider two co-cultures instead of one, which we label as 'habitat patches' A and B. The second crucial addition is the migration step, which occurs after growing the co-cultures for 24 hours and measuring the total population density and relative abundances of the strains, but before dilution into fresh media. In this step, we transfer a fraction m of the cells from each co-culture into the other (corresponding to a fixed volume). The mixed co-cultures are then diluted into fresh media with antibiotics and grown again for 24 hours, as done previously for individual co-cultures. This migration scheme allows us to vary the migration rate over several orders of magnitude, enabling us to experimentally probe the effect of migration on population dynamics, in a systematic manner.

Since migration is known to lead to in-phase synchronization in a variety of systems (13, 16, 21–23), we first quantified the minimum migration rate necessary for the onset of synchronization under benign environmental conditions (10 μg/ml ampicillin, 8 μg/ml chloramphenicol), in which the system exhibits stable oscillations (Fig. 2C). For each migration rate, we performed daily growth-migration-dilution experiments with three initial relative abundances of AmpR to ChlR cells for each of two biological replicates, i.e. a total of six replicate pairs of co-cultures. We observe that while in-phase synchronization can sometimes be observed even at very low migration rates, all replicates showed in-phase synchronization for $m \geq 0.2$ (Fig. 3B). This strongly suggests that the onset of complete in-phase synchronization lies in the region $0.1 < m \leq 0.2$.

While synchronization is certainly an important effect, it is not clear whether it is the only effect that migration has on population dynamics. In particular, it is worth investigating whether there are additional qualitative differences in population oscillations at intermediate migration rates. To this end, we took a closer look at the population time series data as a function of increasing migration rate. It is evident that our coupled co-cultures exhibit period 3 oscillations in the absence of migration ($m = 0$, Fig. 3C) as well as very high migration rates ($m = 0.2$, Fig. 3E),

the difference being that the oscillations are unsynchronized in the former case and in-phase synchronized in the latter. However, the period-3 oscillations are perturbed at intermediate migration rates, and we see signatures of other periods, such as period-4 oscillations at $m = 0.1$ (Fig. 3D). The perturbed oscillations may also reflect the presence of long transients (32). Interestingly, perturbed oscillations appear to be quite common for $m = 0.04$ and $m = 0.1$ but are not observed at very low or very high migration rates (Fig. S1).

The data in Fig. 3C-E demonstrate that migration not only synchronizes population dynamics but also alters them in a qualitative manner. To better understand the sequence of experimental outcomes with increasing migration rate, we turned to an ordinary differential equation based mechanistic model that simulates antibiotic degradation and cell growth. This model was developed in the context of isolated co-cultures and has been shown to reproduce the observed period-3 limit cycle oscillations over a reasonably broad parameter regime (31). The model has two variables N_1 and N_2 corresponding to the population densities of AmpR and ChlR, respectively, and two variables A_1 and A_2 corresponding to the concentrations of the antibiotics ampicillin and chloramphenicol, respectively. Over the 24 hour growth period, the population densities and antibiotic concentrations change with time according to the following equations:

$$\frac{dN_1}{dt} = \gamma_1(A_2)N_1\left(1 - \frac{N_1 + N_2}{K}\right)$$
$$\frac{dN_2}{dt} = \gamma_2(A_1)N_2\left(1 - \frac{N_1 + N_2}{K}\right)$$
$$\frac{dA_1}{dt} = \frac{-V_{max}A_1}{K_m + A_1}N_1(t = 0)$$
$$\frac{dA_2}{dt} = -c_2A_2N_2$$

Here, we assume that bacterial growth is logistic, with antibiotic concentration-dependent growth rates $\gamma_1(A_2)$ and $\gamma_2(A_1)$. The two strains exhibit neutral resource competition, as reflected in the combined carrying capacity K. Ampicillin degradation is assumed to obey Michaelis-Menten kinetics. In reality, ampicillin is degraded by β-lactamase (33, 34) molecules produced by AmpR cells during their growth as well as the free ones carried over from the previous day. Our model

assumes that the dominant contribution comes from the β-lactamases carried over from the previous day. Since the number of enzyme molecules carried over is proportional to the number of AmpR cells present at the beginning of the day, the equation for A_1contains the initial density of AmpR cells $N_1(t=0)$ rather than their instantaneous density $N_1(t)$. Since chloramphenicol degradation is intracellular (33), the degradation rate of chloramphenicol is taken to be proportional to the density of ChlR cells. Finally, since AmpR cells are sensitive to chloramphenicol, and ChlR cells are sensitive to ampicillin, the growth rates of the two strains are proportional to the concentration of the antibiotic to which they are sensitive. These growth rates are given by:

$$\gamma_1(A_2) = \begin{cases} 0 & t < t_{lag} \\ \dfrac{\gamma_1^R}{1 + A_2/I_{12}} & t \geq t_{lag} \end{cases}$$

$$\gamma_2(A_1) = \begin{cases} 0 & t < t_{lag} \\ -\gamma_2^D + \dfrac{\gamma_2^R + \gamma_2^D}{1 + A_1/I_{21}} & t \geq t_{lag} \end{cases}$$

Here, we have also incorporated a lag phase, characterized by a time scale t_{lag} over which the cells do not grow or die. Since chloramphenicol is a bacteriostatic antibiotic, i.e. it inhibits sensitive cell growth but does not cause the cells to die, the growth rate of AmpR cells approaches zero at high concentrations of chloramphenicol but never becomes negative (Fig. 4A, green curve). On the other hand, ampicillin is bactericidal, i.e. its presence can cause sensitive cells to die and we therefore model the growth rate of ChlR cells such that it is negative at high concentrations of ampicillin (Fig. 4A, purple curve). Numerical values and descriptions of all parameters used in the simulations are listed in Table S1. In a typical simulation over a 24 hour growth cycle, the cell densities saturate (Fig. 4B, top panel) and the antibiotics are inactivated (Fig. 4B, bottom panel). We note that the initial and final densities of AmpR and ChR can be substantially different, such that the ratio N_1/N_2 can vary substantially from day to day.

To gain insight into the experimentally observed changes in oscillatory dynamics with increasing migration rate, we implemented the growth-migration-dilution scheme in our simulations. The

chief advantage of simulations is that they allow us to analyze the system's behavior over timescales that are much longer than those accessible in our experiments. The long timescales enable us to discern whether a given dynamical outcome corresponds to stable oscillations or transient dynamics. Simulations also facilitate a detailed characterization of oscillatory dynamics as well as the range of migration rates over which they are observed. In our simulations, we started with two patches A and B for which we numerically integrated the model equations over 24 hours. To implement the migration and dilution steps, we mimicked the experimental protocol by resetting the initial population densities and antibiotic concentrations in the two patches for the next day of growth in accordance with the dilution factor of 100 and the migration rate m. The system's dynamical outcomes are best summarized in the form of a bifurcation diagram as a function of the migration rate (Fig. 4C). In this bifurcation diagram we have plotted the unique values attained by the population, i.e. the ratio of AmpR to ChlR cells in patch A over the last 50 days of a simulation consisting of 1000 daily dilution cycles.

As expected, we observe a regime of period-3 oscillations at very low migration rates (Fig. 4C, blue region) as well as high migration rates (Fig. 4C, red region). Moreover, these oscillations are unsynchronized at very low migration rates and synchronized in-phase at high migration rates (Fig. 4C, insets corresponding to blue and red regions). Quite remarkably, the bifurcation diagram also contains a regime of period-4 limit cycle oscillations (Fig. 4C, orange region and inset) at intermediate migration rates that is surrounded on both sides by narrow regions characterized by irregular dynamics and long transients (Fig. 4C, green regions). The dynamics in these regions are strikingly similar to the perturbed oscillations observed in our experiments (Fig. 3D and Fig. S1). Indeed, our simple model successfully captures the sequence of experimentally observed dynamical outcomes as a function of the migration rate. In particular, transitions between different dynamical regimes are in reasonable qualitative agreement with our experiments. Moreover, the presence of altered population dynamics in both experiments and simulations suggests that intermediate migration rates can indeed give rise to population dynamics that are distinct from those in the uncoupled and synchronized regimes.

It is plausible that the disturbance of oscillations at intermediate migration rates may influence a population's viability in harsh environments, although it is not *a priori* obvious whether this

influence would be harmful or beneficial. As mentioned earlier, it has been suggested that synchronization can enhance the risk of global extinction in harsh environments (13, 16), which implies that high migration rates may have a deleterious impact on the probability of survival, but it is not clear if this effect is monotonic. To explore the effect of intermediate migration rates on survival probability, we simulated our model in harsh environmental conditions. For these simulations, a harsh environment corresponds to higher antibiotic concentrations (10 μg/ml ampicillin, 16 μg/ml chloramphenicol), where the model predicts that isolated populations go extinct deterministically in the absence of migration. Furthermore, we introduce 15% noise in the migration and dilution steps of our simulations, to mimic the stochastic fluctuations resulting from our experimental protocol. To quantify the impact of migration on survival, we generated probability distributions $P(\tau)$ of population lifetimes, i.e. the durations τ for which the populations survived for various m (Fig. 5A). The distributions decay exponentially over a timescale that increases with migration rate for $m \lesssim 0.03$ and decrease with migration rate for $m \gtrsim 0.1$. Interestingly, within a narrow intermediate migration regime ($0.04 \lesssim m \lesssim 0.07$), the survival time distributions have longer tails, which suggests that intermediate migration rates can result in enhanced survival as compared with isolated populations or strongly coupled ones. Overall, the variation of $P(\tau)$ with m indicates that moderate levels of migration offer the best chance of survival in harsh conditions.

A more experimentally tractable measure of the effect of migration on survival in challenging environments is the fraction of populations that survive over a given period of time. Towards this end, we computed the probability of survival over 10 days. As expected from the variation in $P(\tau)$ with m (Fig. 5A), the survival probability over 10 days changes non-monotonically with the migration rate (Fig. 5B). This qualitative trend is independent of the duration over which survival probability is computed (Fig. S2). Moreover, the peak in survival probability occurs in the regime where we observe a double exponential decay in $P(\tau)$, once again suggesting that moderate levels of migration perturb population dynamics in a manner that favors extended survival.

Motivated by the simulation results, we proceeded to test whether the predicted non-monotonicity of survival probability with m is also observed in experiments. Accordingly, we

298 performed growth-dilution-migration experiments with higher antibiotic concentrations (10
299 μg/ml ampicillin, 16 μg/ml chloramphenicol) and measured the fraction of populations that
300 survived over 10 days. As predicted by the simulations, the survival probability indeed shows a
301 peak at intermediate migration rates (Fig. 5C. See Fig. S3 for population density time series).
302 Further, the location of the maximum shows reasonably good quantitative agreement with the
303 simulations. Collectively, these findings establish that moderate levels of migration promote
304 population dynamics that extended survival in harsh environments.
305
306 **Discussion:**
307 Here, we have shown that two oscillating bacterial populations can synchronize when coupled
308 sufficiently strongly via migration. Furthermore, we have demonstrated that it is possible for the
309 migration rate itself to determine the period of oscillation. In particular, our experimental system
310 exhibits limit cycle period-3 oscillations in the absence of migration. However, we observed
311 disturbances in these dynamics in the presence of migration that were consistent with the period-
312 4 oscillations predicted by the model at intermediate migration rates (Fig. 3D). This finding
313 suggests that the characteristics of population oscillations observed in nature may not simply be a
314 result of intrinsic inter- or intra-species interactions, but may also be a consequence of spatial
315 structure and migration.
316
317 Since migration can perturb population dynamics, it also has the potential to influence the
318 survival of a population in a challenging environment. For instance, we found that populations
319 were most likely to survive the duration of the experiment at intermediate migration rates (Fig.
320 5). The presence of a maximum in survival probability at intermediate migration rates is
321 potentially relevant in conservation biology and epidemiology in that controlling migration
322 might lead to desired outcomes like population stability or disease eradication. Interestingly, the
323 dynamics we observe within this intermediate migration rate regime resemble noisy out-of-phase
324 period-2 oscillations (see Fig. S4 for bifurcation diagrams and a representative time series), and
325 we see signatures of such oscillations in some of our surviving experimental populations as well
326 (Fig. S5). Intuitively, out-of-phase synchronization could ensure that the populations in the two
327 patches do not simultaneously become low, which averts the danger of global extinction. In
328 previous computational studies (30, 35–37), such out-of-phase synchronization has been widely

recognized as a potential mechanism for survival and our experiments provide direct evidence in support of these numerical findings.

In field ecology and metapopulation theory, re-colonization of habitat patches after local extinction events is thought to be a major contributor to extended survival in harsh environments (8), a claim supported by recent experiments on protists (10). However, we observed relatively few instances of such re-colonization (Fig. S6), implying that re-colonization is not the major cause of extended survival in our system. Nevertheless, in a more spatially extended population with a larger number of possible habitats, it may be possible that re-colonization plays a more significant role in enabling populations to survive in challenging conditions.

Finally, we note that in challenging environments, evolutionary rescue can also lead to population recovery (38). In our system, evolutionary rescue may occur either via enhanced antibiotic tolerance through the evolution of lag time mutants (39) or via increased drug resistance in one of the strains. Indeed, we did observe a few cases in which ChlR cells developed a higher resistance to ampicillin, particularly at high migration rates in the harsh environment (10 μg/ml ampicillin, 16 μg/ml chloramphenicol) (Fig. S7). Interestingly, we found no evidence of such evolution in extremely harsh environments (10 μg/ml ampicillin, 20 μg/ml chloramphenicol), in which all populations became extinct within 7 days (Fig. S8). Collectively, these observations suggest that the optimal conditions for evolution of additional antibiotic resistance represent a tradeoff between selection pressure, which is primarily determined by the environment, and survival time, which can be influenced by the migration rate. In addition, the effective population size may also play a role in guiding the course of evolution in that stronger coupling may lead to a larger population size and thus more genetic diversity, but may also lead to reduced survival time.

In the present study, we found that moderate amounts of migration between two coupled bacterial populations can significantly perturb population oscillations, and enhance survival in harsh environments (Fig. 3D-E). While these findings are directly relevant to the ecology of spatially extended populations, they may also have implications for a variety of coupled biological oscillations such as those observed in the flashing of fireflies (40), the spread of

infectious diseases (21–23), and the quorum sensing-mediated lysis of engineered bacteria (41). In the future, it would be interesting to extend our findings to networks with more than two populations, where in addition to the migration rate, the network topology plays an important role in governing synchronization (27, 42). The network topology also allows exotic forms of partial synchronization such as phase clusters and chimeras (43–45), whose relevance to ecological systems is hitherto unexplored. The effects of asymmetric migration rates, spatial expansion, and environmental conditions are also worthy of exploration (35, 46–48). More generally, our experiments lay the foundation for a bottom-up approach aimed at unraveling key aspects of population dynamics on the complex networks encountered in conservation biology and epidemiology.

Materials and Methods:

Strains: The strains used are identical to those in (31). Briefly, the chloramphenicol-resistant strain ChlR is an *E. coli* DH5α strain transformed with the pBbS5c-RFP plasmid (49) which encodes a gene for chloramphenicol acetyltransferase (type I) enzyme as well as a gene for monomeric red fluorescent protein (RFP). The plasmid pbBS5c-RFP was obtained from Jay Keasling (University of California, Berkeley, CA) via Addgene (plasmid 35284) (49). The ampicillin-resistant strain is an *E. coli* DH5α strain transformed with a plasmid encoding a gene for the β-lactamase enzyme (TEM-1) and a gene for enhanced yellow fluorescent protein (EYFP).

Experiments: Initial monocultures of our strains were grown for 24 h in culture tubes containing 5 ml LB supplemented with antibiotic for selection (50 μg/mL ampicillin and 25 μg/mL chloramphenicol for AmpR and ChlR, respectively) at 37°C and shaken at 250 rpm. The following day, 200 μL of co-cultures of the two strains were grown at varying initial population fractions in LB without antibiotics. For synchronization experiments, the initial ratios of AmpR cells to ChlR cells were chosen such that the probability for paired co-cultures to be in the same phase of oscillation in the absence of migration ($m = 0$) was low. Subsequently, serial migration-dilution experiments were performed in well-mixed batch culture with a culture volume of 200 μL. In each cycle, co-cultures were grown for 24 hours in LB media supplemented with the antibiotics ampicillin and chloramphenicol. During growth, cultures were

shaken at 500 rpm at a temperature of 37°C. At the end of the growth cycle, we measured the optical density (OD) at 600 nm and prepared flow cytometry samples by diluting 5μL of each grown co-culture by a factor of 1600 into phosphate buffer (PBS, Corning 21-040-CV). To perform the migration step, we pipetted fixed volumes of each co-culture within a connected pair into the other at the end of each growth cycle; subsequently, these co-cultures were diluted by a factor of 100 into fresh LB media and antibiotics. Growth medium was prepared by using BD's Difco TM LB Broth (Miller) (catalog no. 244620). Ampicillin stock was prepared by dissolving ampicillin sodium salt (Sigma-Aldrich catalog no. A9518) in LB at a concentration of 50 mg/mL. The solution was filter sterilized, stored frozen at −20°C, and thawed before use. Chloramphenicol stock was prepared by dissolving chloramphenicol powder (Sigma-Aldrich catalog no. C0378) in 200 proof pure ethanol (KOPTEC) at a concentration of 25 mg/mL. This solution was filter sterilized and stored at −20°C. Prepared 96-well plates of media supplemented with antibiotics were stored at −80°C, thawed 1 d prior to inoculation at 4°C and warmed for 1hour at 37°C immediately before inoculation.

Measurement and Data Analysis: At the end of each growth cycle, we took spectrophotometric (Thermo Scientific Varioskan Flash at 600 nm) measurements, which serve as a proxy for the total population size. We converted the OD measurement to CFU/μl based on a calibration curve obtained from counting colonies on LB and agar plates originating from cultures at various cell densities. We also took flow cytometry (Miltenyi Biotec MACSQuant VYB) measurements of the cultures to determine subpopulation sizes. We consider two populations to be synchronized in-phase if the peaks of their oscillation occur at the same time over the last two oscillation cycles (the final 40% of the experiment), to reduce the influence of transients as well as gather sufficient statistics. Data analysis was performed using a combination of Matlab and Origin. Simulations were performed using Matlab. Flow cytometry data were analyzed using the Python package FlowCytometryTools (50). Data are available upon request.

Acknowledgements:

This work was primarily supported by NIH Grant R01 GM102311-01 and National Science Foundation CAREER Award PHY-1055154. The laboratory acknowledges support from the Pew Scholars in the Biomedical Sciences Program Grant 2010-000224-007, NIH R00 Pathways

to Independence Award GM085279-02, Sloan Foundation Fellowship BR2011-066, the Allen Distinguished Investigator Program, and NIH New Innovator Award DP2. S.G. was supported by a Human Frontier Science Program cross-disciplinary postdoctoral fellowship. We also thank members of the Gore Lab for helpful discussions.

References:

1. Gilpin M (2012) *Metapopulation dynamics: empirical and theoretical investigations* (Academic Press).

2. Guimera R, Mossa S, Turtschi A, Amaral LN (2005) The worldwide air transportation network: Anomalous centrality, community structure, and cities' global roles. *Proc Natl Acad Sci USA* 102(22):7794–7799.

3. Hanski I (1998) Metapopulation dynamics. *Nature* 396(6706):41.

4. Blasius B, Huppert A, Stone L (1999) Complex dynamics and phase synchronization in spatially extended ecological systems. *Nature* 399(6734):354.

5. Dey S, Joshi A (2006) Stability via asynchrony in Drosophila metapopulations with low migration rates. *Science* 312(5772):434–436.

6. Molofsky J, Ferdy J-B (2005) Extinction dynamics in experimental metapopulations. *Proc Natl Acad Sci USA* 102(10):3726–3731.

7. Abbott KC (2011) A dispersal-induced paradox: synchrony and stability in stochastic metapopulations. *Ecol Lett* 14(11):1158–1169.

8. Harrison S (1991) Local extinction in a metapopulation context: an empirical evaluation. *Biol J Linn Soc* 42(1–2):73–88.

9. Gonzalez A, Lawton JH, Gilbert FS, Blackburn TM, Evans-Freke I (1998) Metapopulation dynamics, abundance, and distribution in a microecosystem. *Science* 281(5385):2045–2047.

10. Fox JW, Vasseur D, Cotroneo M, Guan L, Simon F (2017) Population extinctions can increase metapopulation persistence. *Nat Ecol Evol* 1(9):1271.

11. Hilty JA, Lidicker Jr WZ, Merenlender A (2012) *Corridor ecology: the science and practice of linking landscapes for biodiversity conservation* (Island Press).

12. Liebhold A, Koenig WD, Bjørnstad ON (2004) Spatial synchrony in population dynamics. *Annu Rev Ecol Evol Syst* 35:467–490.

13. Earn DJ, Levin SA, Rohani P (2000) Coherence and conservation. *Science* 290(5495):1360–1364.

14. Ray C, Hastings A (1996) Density dependence: are we searching at the wrong spatial scale? *J Anim Ecol*:556–566.

15. Odum EP, ODUM H (1953) Fundamentals of ecology. 1953. *Fundam Ecol Philadephie Saunders*.

16. Kerr B, Neuhauser C, Bohannan BJ, Dean AM (2006) Local migration promotes competitive restraint in a host-pathogen'tragedy of the commons'. *Nature* 442(7098):75.

17. Nathan R (2006) Long-distance dispersal of plants. *Science* 313(5788):786–788.

18. Alldredge AL, Silver MW (1988) Characteristics, dynamics and significance of marine snow. *Prog Oceanogr* 20(1):41–82.

19. Azam F, Long RA (2001) Sea snow microcosms. *Nature* 414(6863):495–498.

20. Tatem AJ, Rogers DJ, Hay SI (2006) Global transport networks and infectious disease spread. *Adv Parasitol* 62:293–343.

21. Grassly NC, Fraser C, Garnett GP (2005) Host immunity and synchronized epidemics of syphilis across the United States. *Nature* 433(7024):417.

22. Grenfell BT, Bjørnstad ON, Kappey J (2001) Travelling waves and spatial hierarchies in measles epidemics. *Nature* 414(6865):716–723.

23. Viboud C, et al. (2006) Synchrony, waves, and spatial hierarchies in the spread of influenza. *Science* 312(5772):447–451.

24. Earn DJ, Rohani P, Grenfell BT (1998) Persistence, chaos and synchrony in ecology and epidemiology. *Proc R Soc Lond B Biol Sci* 265(1390):7–10.

25. Rohani P, Earn DJ, Grenfell BT (1999) Opposite patterns of synchrony in sympatric disease metapopulations. *Science* 286(5441):968–971.

26. Earn DJ, Levin SA (2006) Global asymptotic coherence in discrete dynamical systems. *Proc Natl Acad Sci USA* 103(11):3968–3971.

27. Noble AE, Machta J, Hastings A (2015) Emergent long-range synchronization of oscillating ecological populations without external forcing described by Ising universality. *Nat Commun* 6.

28. Gyllenberg M, Söderbacka G, Ericsson S (1993) Does migration stabilize local population dynamics? Analysis of a discrete metapopulation model. *Math Biosci* 118(1):25–49.

29. Hastings A (1993) Complex interactions between dispersal and dynamics: lessons from coupled logistic equations. *Ecology* 74(5):1362–1372.

30. Zion YB, Yaari G, Shnerb NM (2010) Optimizing metapopulation sustainability through a checkerboard strategy. *PLoS Comput Biol* 6(1):e1000643.

31. Yurtsev EA, Conwill A, Gore J (2016) Oscillatory dynamics in a bacterial cross-protection mutualism. *Proc Natl Acad Sci USA* 113(22):6236–6241.

32. Wysham DB, Hastings A (2008) Sudden shifts in ecological systems: Intermittency and transients in the coupled Ricker population model. *Bull Math Biol* 70(4):1013–1031.

33. Nicoloff H, Andersson DI (2015) Indirect resistance to several classes of antibiotics in cocultures with resistant bacteria expressing antibiotic-modifying or-degrading enzymes. *J Antimicrob Chemother* 71(1):100–110.

34. Sykes RB, Matthew M (1976) The β-lactamases of gram-negative bacteria and their role in resistance to β-lactam antibiotics. *J Antimicrob Chemother* 2(2):115–157.

35. Dey S, Goswami B, Joshi A (2014) Effects of symmetric and asymmetric dispersal on the dynamics of heterogeneous metapopulations: two-patch systems revisited. *J Theor Biol* 345:52–60.

36. Dey S, Goswami B, Joshi A (2015) A possible mechanism for the attainment of out-of-phase periodic dynamics in two chaotic subpopulations coupled at low dispersal rate. *J Theor Biol* 367:100–110.

37. Ben-Zion Y, Fried Y, Shnerb NM (2012) Migration, coherence and persistence in a fragmented landscape. *Theor Ecol* 5(4):481–493.

38. Bell G, Gonzalez A (2011) Adaptation and evolutionary rescue in metapopulations experiencing environmental deterioration. *Science* 332(6035):1327–1330.

39. Fridman O, Goldberg A, Ronin I, Shoresh N, Balaban NQ (2014) Optimization of lag time underlies antibiotic tolerance in evolved bacterial populations. *Nature* 513(7518):418.

40. Moiseff A, Copeland J (2010) Firefly synchrony: a behavioral strategy to minimize visual clutter. *Science* 329(5988):181–181.

41. Danino T, Mondragon-Palomino O, Tsimring L, Hasty J (2010) A synchronized quorum of genetic clocks. *Nature* 463(7279):326.

42. Holland MD, Hastings A (2008) Strong effect of dispersal network structure on ecological dynamics. *Nature* 456(7223):792.

43. Abrams DM, Strogatz SH (2004) Chimera states for coupled oscillators. *Phys Rev Lett* 93(17):174102.

44. Tinsley MR, Nkomo S, Showalter K (2012) Chimera and phase-cluster states in populations of coupled chemical oscillators. *Nat Phys* 8(9):662.

513 45. Martens EA, Thutupalli S, Fourrière A, Hallatschek O (2013) Chimera states in mechanical
514 oscillator networks. *Proc Natl Acad Sci USA* 110(26):10563–10567.

515 46. Franco D, Ruiz-Herrera A (2015) To connect or not to connect isolated patches. *J Theor Biol*
516 370:72–80.

517 47. Becks L, Arndt H (2013) Different types of synchrony in chaotic and cyclic communities. *Nat*
518 *Commun* 4:1359.

519 48. Sullivan LL, Li B, Miller TE, Neubert MG, Shaw AK (2017) Density dependence in demography and
520 dispersal generates fluctuating invasion speeds. *Proc Natl Acad Sci USA* 114(19):5053–5058.

521 49. Lee TS, et al. (2011) BglBrick vectors and datasheets: a synthetic biology platform for gene
522 expression. *J Biol Eng* 5(1):12.

523 50. Yurtsev E, Friedman J, Gore J *FlowCytometryTools: Version 0.4.5*, doi 10.5281/zenodo.32991.

524

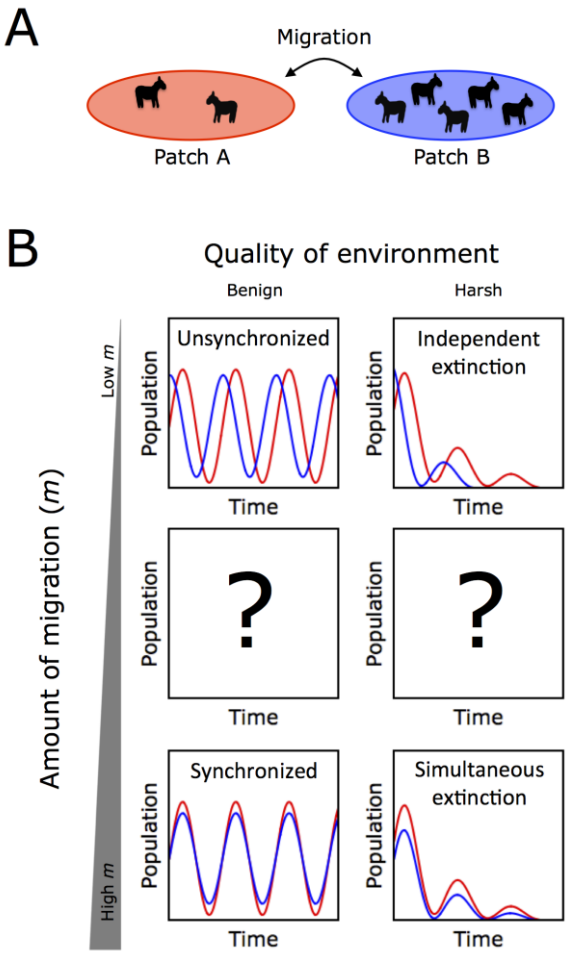

Fig 1: The cartoon illustrates possible qualitative effects of migration on population dynamics of a species in benign as well as harsh environmental conditions. A) The population dynamics of two patches can be coupled via migration. **B)** Under benign conditions, low migration rates are insufficient to couple population dynamics on the two patches (top left). On the other hand, high migration rates lead to in-phase synchronization, rendering the two patches equivalent (bottom left). An open question concerns how the population dynamics respond to intermediate migration rates (center left). In harsh conditions, population patches can become extinct (top right) and high migrations rate could lead to simultaneous extinction (bottom right). At intermediate migration rates, we investigate whether altered population dynamics could potentially lead to longer survival times (center right).

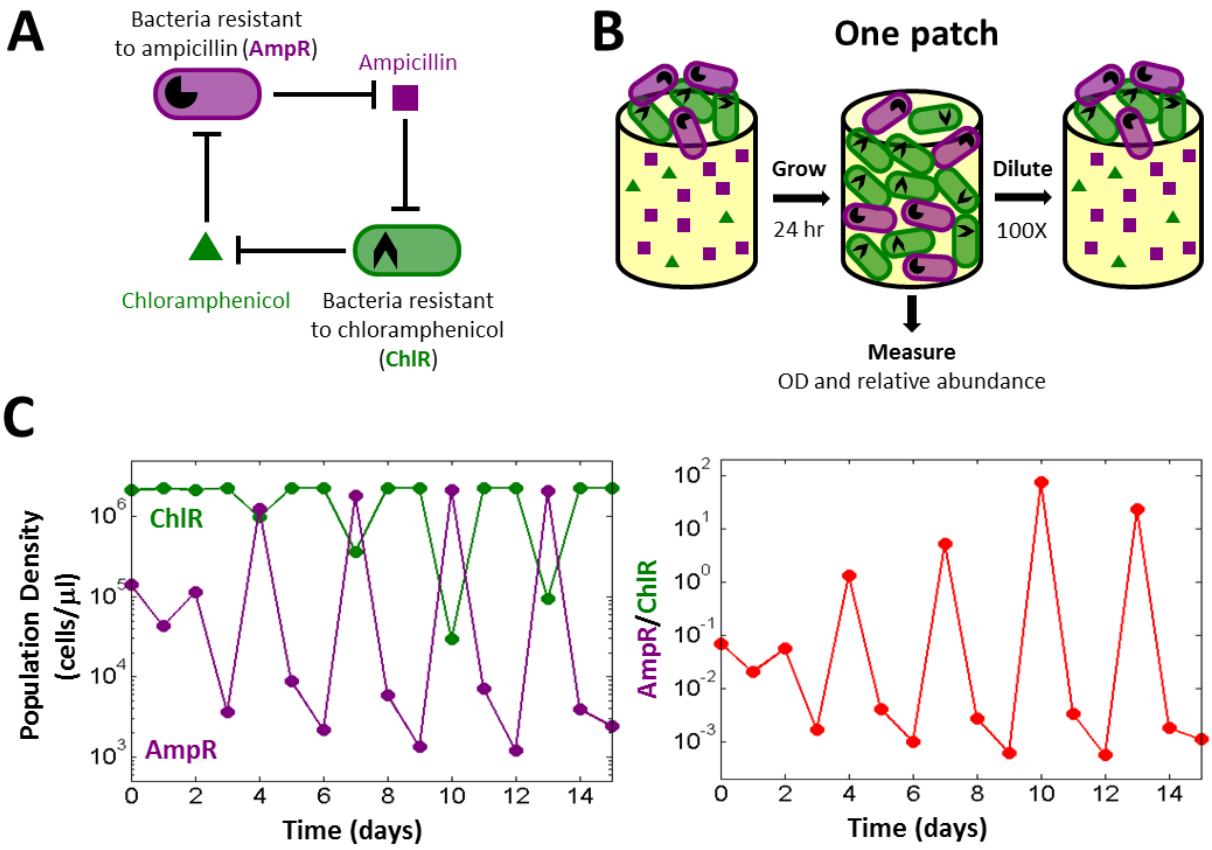

Fig 2: A bacterial cross-protection mutualism serves as a model system to study migration-induced synchronization of population oscillations. A) Diagram depicting the mutualistic interaction between ampicillin resistant (AmpR) and chloramphenicol resistant (ChlR) cells. AmpR cells protect ChlR cells by enzymatically deactivating ampicillin, whereas ChlR cells protect AmpR cells by deactivating chloramphenicol. **B)** Schematic illustration of the experimental growth-dilution scheme for growing isolated co-cultures in the absence of migration. Each day, cells are grown for 24 hours and then diluted by a factor of 100 into fresh media and antibiotics. The total cell density as well as relative proportions of AmpR and ChlR cells are measured after 24 hours of growth, before the dilution step. **C)** Isolated co-cultures exhibit period 3 oscillations in the density of AmpR and ChlR cells (left panel) as well as in the ratio of AmpR cells to ChlR cells (right panel) under benign conditions. This experimental condition corresponds to 10 μg/ml of ampicillin and 8 μg/ml of chloramphenicol.

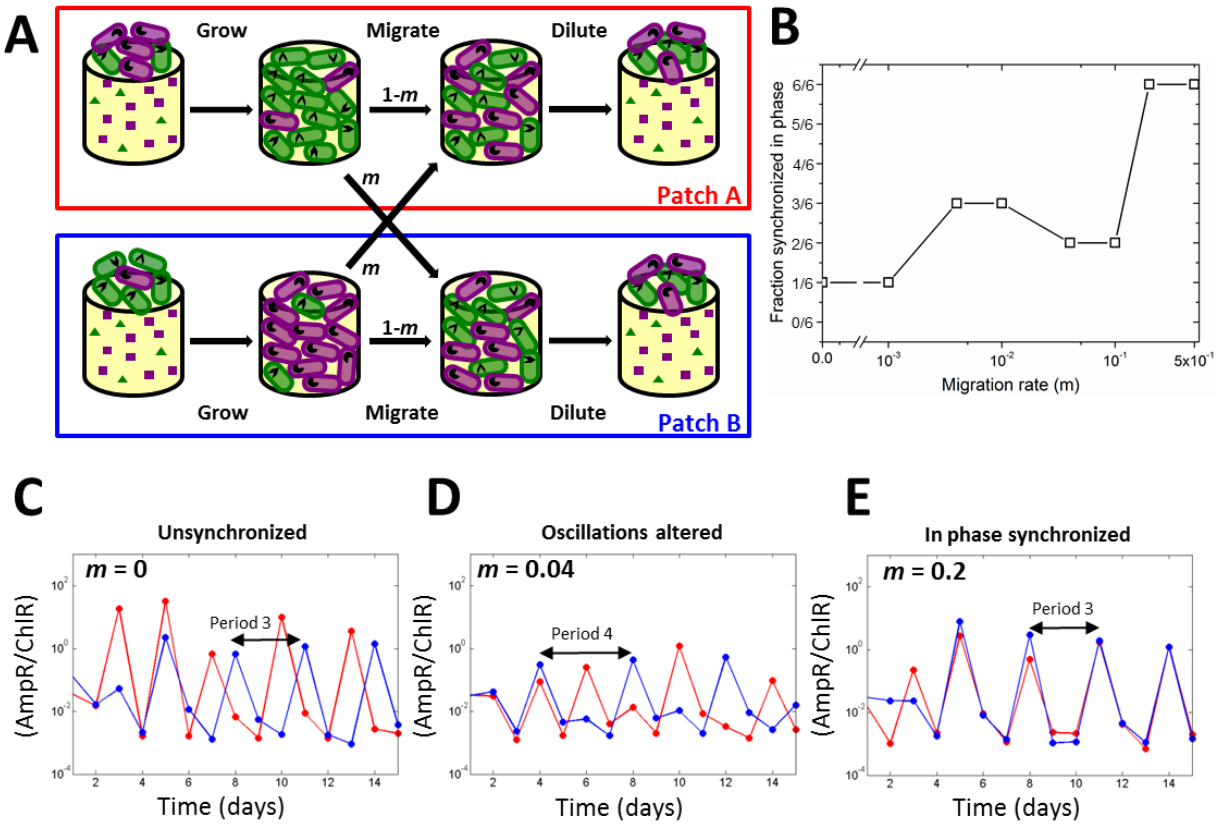

Fig 3: Increased migration rate leads to altered population dynamics and ultimately to synchronization. A) Schematic illustration of the growth-migration-dilution scheme employed in the experiments with two connected bacterial populations. The two patches A (red box) and B (blue box) correspond to two distinct co-cultures of AmpR and ChlR cells. The migration rate is denoted by *m*. **B)** The fraction (out of six replicates) of connected pairs of co-cultures synchronized in phase as a function of the migration rate in benign environmental conditions. **C-E)** Representative time series for the ratio of AmpR cells to ChlR cells in patches A (red plot) and B (blue plot) for $m = 0$ (**C**), $m = 0.04$ (**D**), and $m = 0.2$ (**E**), showing unsynchronized period 3 oscillations, disturbed oscillations with various periods and in-phase synchronized period 3 oscillations respectively. In **B-E**, the experimental condition corresponds to 10 μg/ml of ampicillin and 8 μg/ml of chloramphenicol.

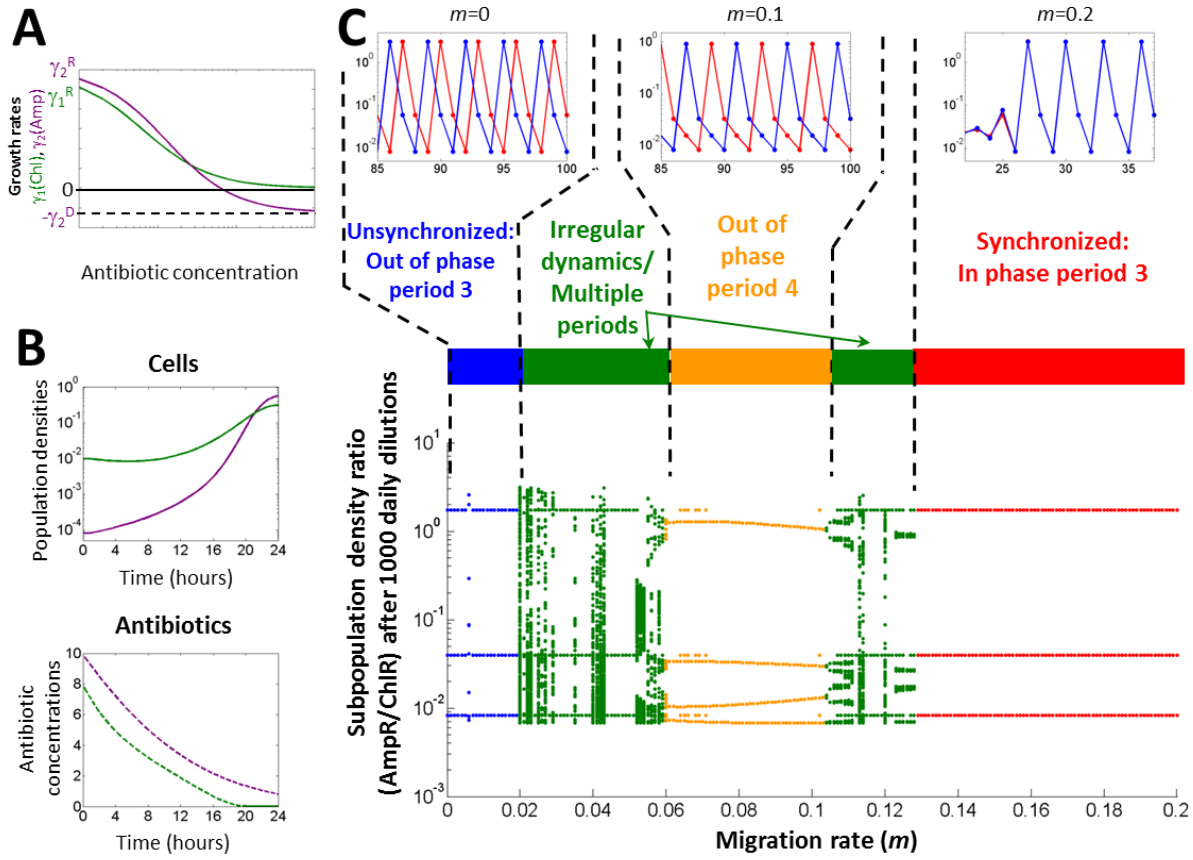

Fig 4: A mechanistic model of antibiotic degradation captures the experimentally observed sequence of dynamical outcomes. A) Dependence of growth rates on the concentration of antibiotics. **B)** Simulated ampicillin resistant (AmpR) and chloramphenicol resistant (ChlR) cell densities (top panel) and antibiotic concentrations (bottom panel) over the course of one 24 hour growth cycle, shown in purple and green respectively. **C)** Bifurcation diagram for a simulation of two co-cultures in a benign environmental condition (10 μg/ml of ampicillin, 8 μg/ml of chloramphenicol) as a function of the migration rate *m*. Unique values of the subpopulation density ratio (AmpR/ChlR) attained by patch A at the end of the growth cycle over the last 50 days of a simulation with 1000 daily dilutions are plotted for each migration rate. The diagram captures the sequence of observed dynamical outcomes: unsynchronized period 3 oscillations in the absence of migration, period-4 oscillations and irregular dynamics at intermediate migration rates, and in-phase synchronized period 3 oscillations at large migration rates. The insets in (C) show representative time series for $m = 0$, $m = 0.1$ and $m = 0.2$. Model parameters can be found in Table S1.

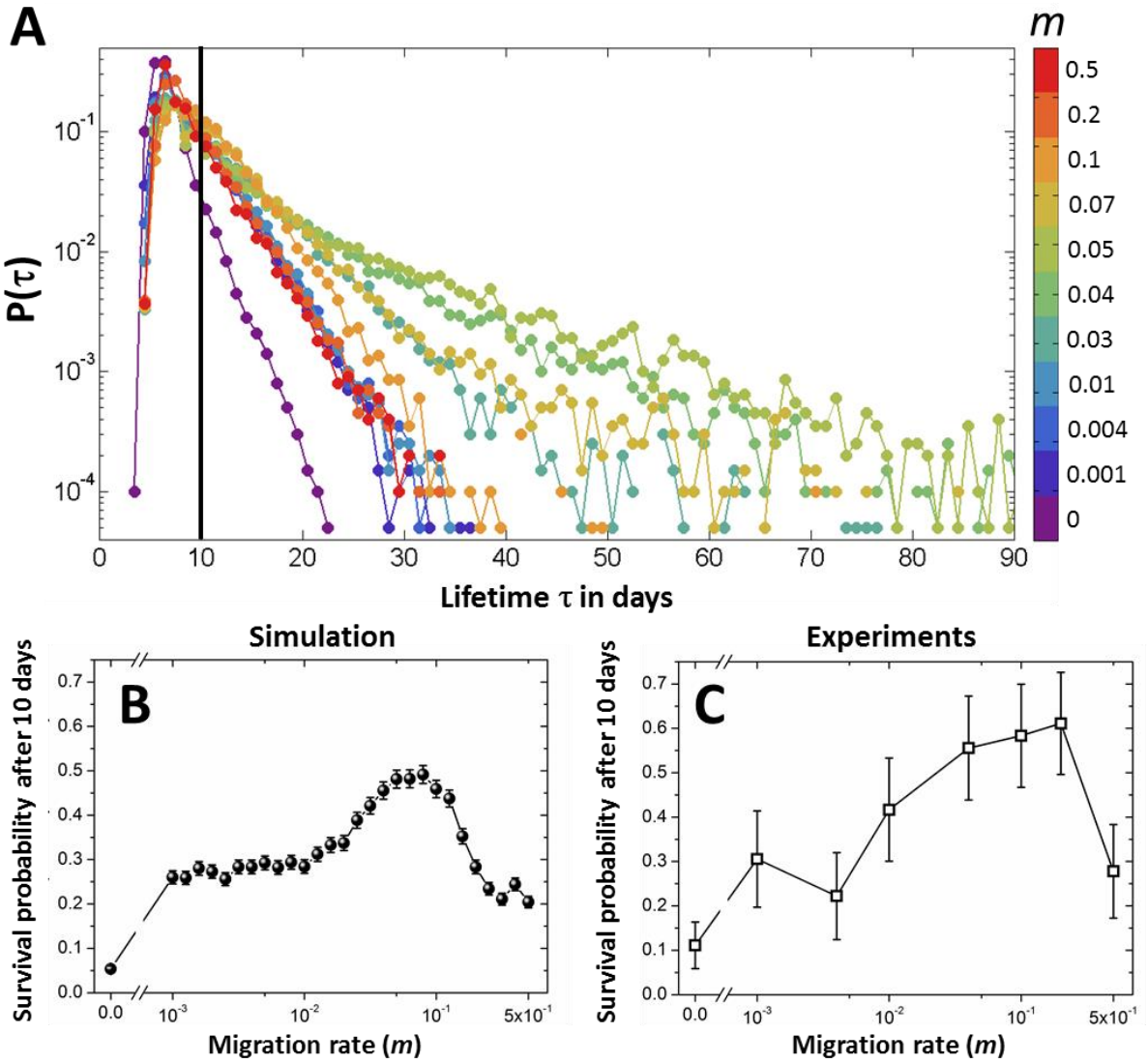

Fig 5: Moderate levels of migration help populations survive longer in harsh environments. **A)** Simulated probability distributions of survival times of populations in a harsh environment (10 μg/ml of ampicillin, 16 μg/ml of chloramphenicol) for various migration rates. The distributions were generated from 6000 simulation runs with initial conditions distributed around the three phases of the period-3 oscillations observed in Fig. 4C. Connected patches were initialized in different phases to avoid minimize synchronization. $P(\tau)$ is defined as the fraction of initial conditions that survived for τ days. Different colors represent different migration rates, as indicated in the colorbar. The survival time distributions have longer tails at intermediate migration rates. The black vertical line indicates the threshold (10 days) used for calculating the

587 survival probability. This threshold was chosen to match the duration of the experiments. **B)**
588 Simulated probability of survival after 10 days in the harsh environment as a function of the
589 migration rate. **C)** Experimentally measured survival probability after 10 days as a function of
590 the migration rate. Both (B) and (C) exhibit a maximum at intermediate migration rates,
591 demonstrating that moderate amounts of migration help populations to survive longer in harsh
592 environments. The error bars in (B) and (C) are standard errors of proportion.

593

Supporting Information

Migration alters oscillatory dynamics and promotes survival in connected bacterial populations

Shreyas Gokhale*, Arolyn Conwill*, Tanvi Ranjan, and Jeff Gore

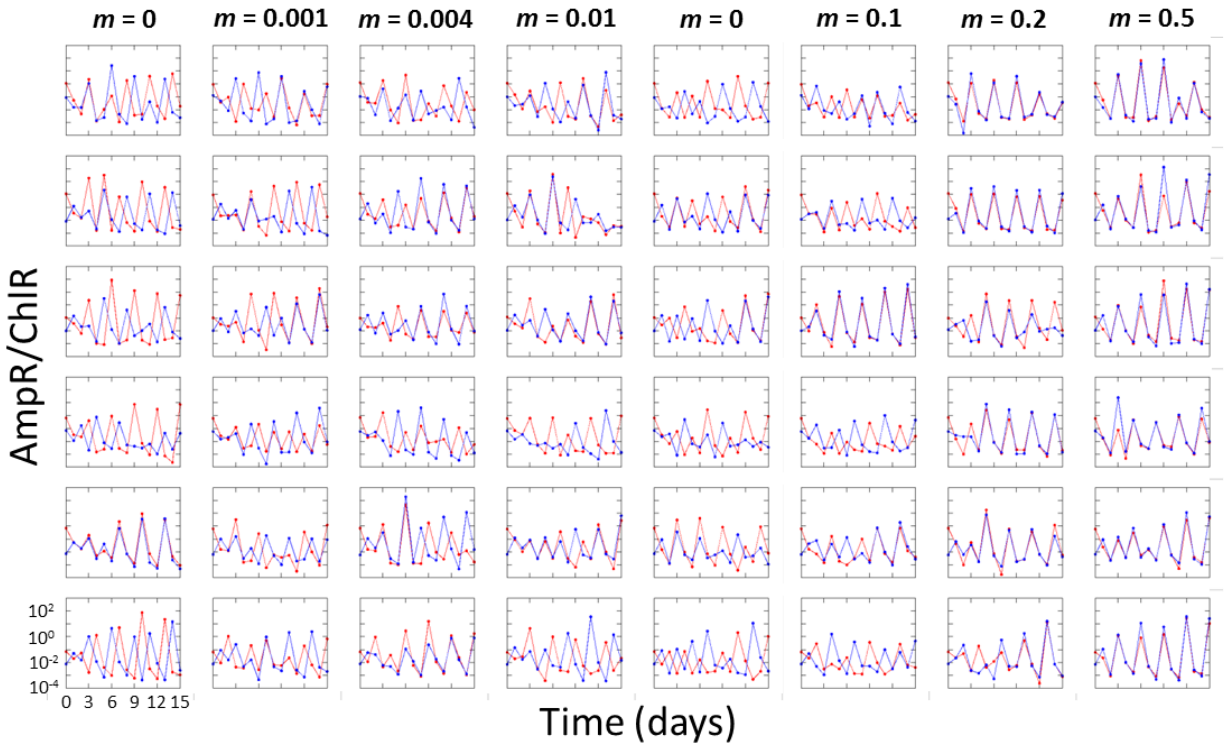

Fig. S1: Time series data for the ratio of AmpR to ChlR cells in two connected population patches in the benign environment (10 μg/ml of ampicillin, 8 μg/ml of chloramphenicol). Each column corresponds to a different migration rate, as shown, and each row corresponds to a different replicate. While some instances of in-phase synchronization are observed at low migration rates, all pairs are synchronized in-phase at $m = 0.2$ and $m = 0.5$. The scales on horizontal and vertical axes are shown at the bottom left.

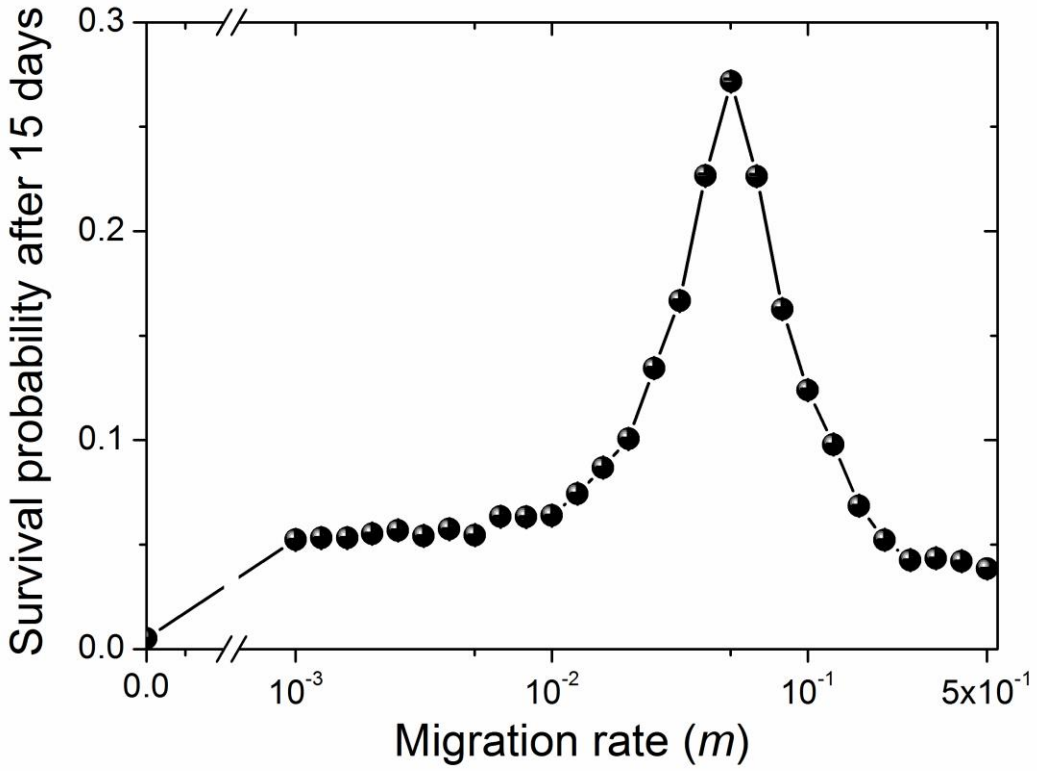

Fig. S2: Simulation data for survival probability after 15 days as a function of migration rate for the harsh environment (10 μg/ml of ampicillin, 16 μg/ml of chloramphenicol), showing a pronounced maximum near $m = 0.05$. The overall survival probability is smaller compared to that measured over 10 days (Fig. 5B in the main text), but the maximum is much sharper. Both the overall decrease in survival probability and the sharpness of the peak are consistent with the simulated distribution of survival times (Fig. 5A in the main text).

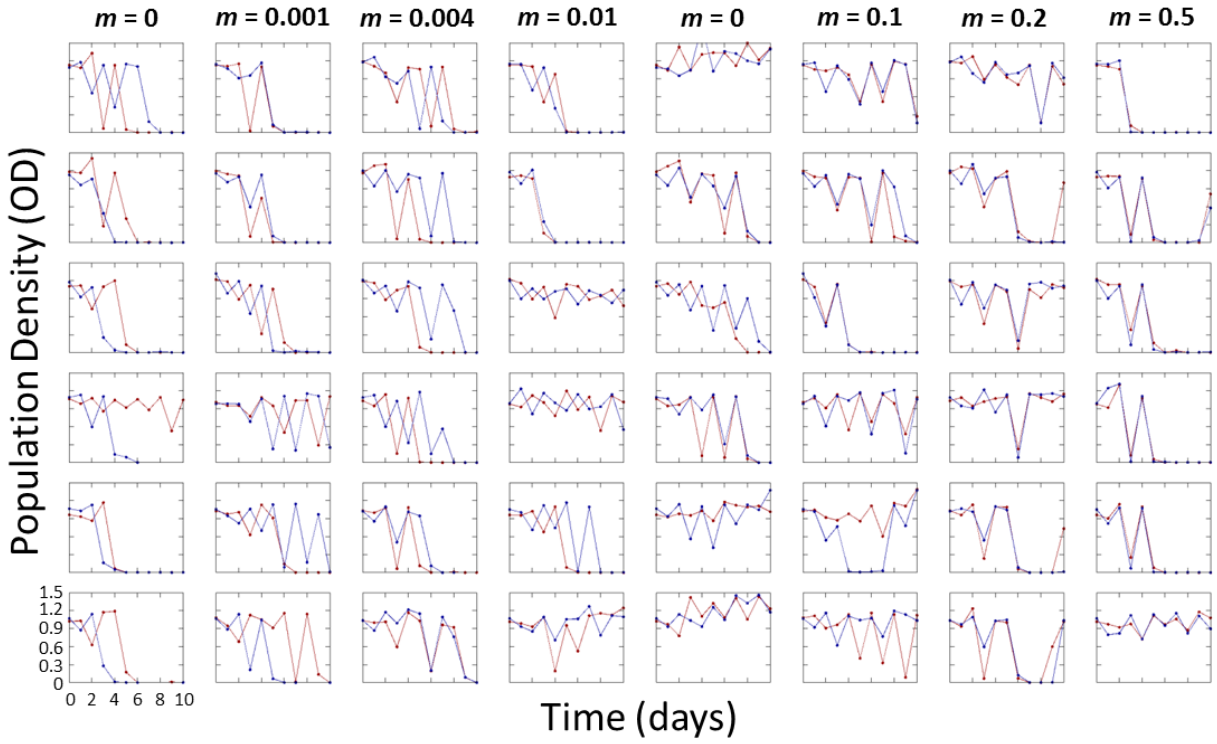

Fig. S3: Time series data for the population density, measured as the optical density (OD) at 600 nm, in the harsh environment (10 μg/ml of ampicillin, 16 μg/ml of chloramphenicol) for six replicates at each of all 8 migration rates studied. The fraction of surviving populations at $m = 0$ and $m = 0.5$ is noticeably smaller compared to that at intermediate migration rates. The scales on horizontal and vertical axes are shown on the bottom left.

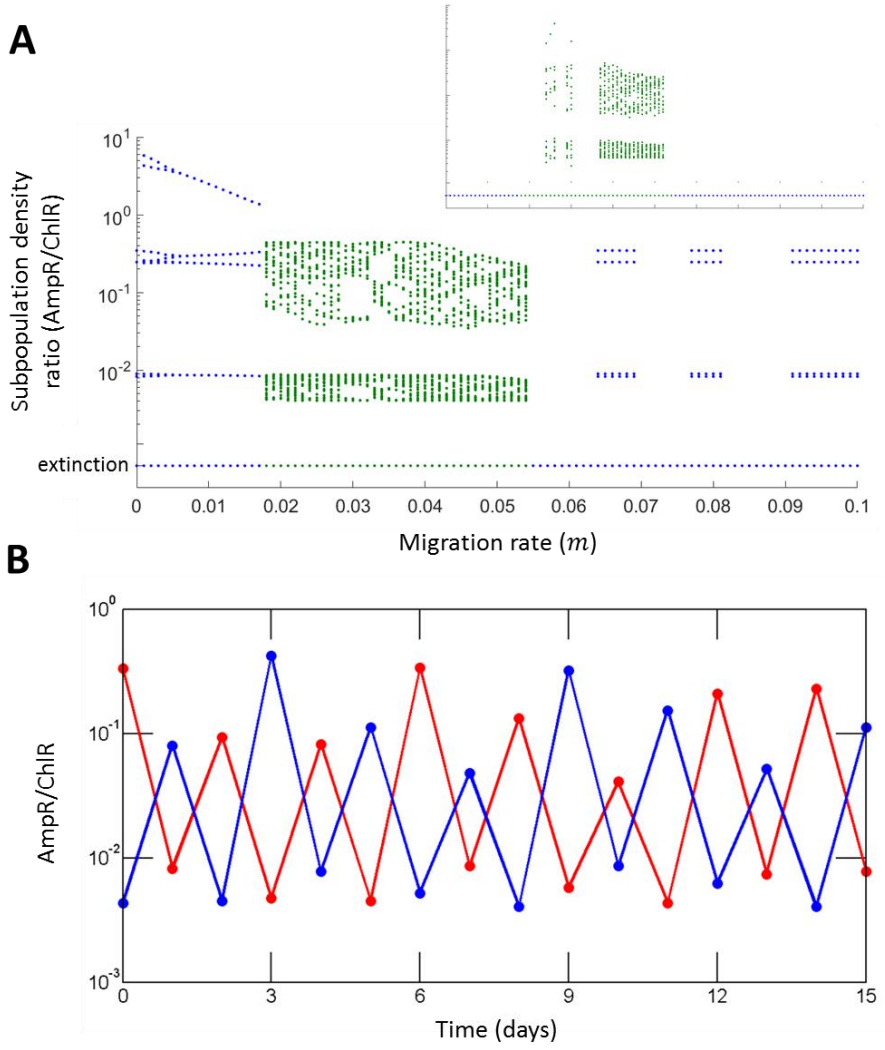

Fig. S4: Simulations reveal the presence of new dynamical states that appear over a narrow range of intermediate migration rates in the harsh environment (10 μg/ml of ampicillin, 16 μg/ml of chloramphenicol). **A)** Bifurcation diagram as a function of migration rate. Unique population values attained by patch A over the last 20 days of a deterministic simulation with 100 daily dilutions are plotted for each migration rate. The simulations were initialized at AmpR/ChlR ratios corresponding to the three phases of the period-3 limit cycle observed in benign conditions. Connected patches were initialized in different phases to minimize the probability of synchronization. Complex dynamics are observed over a narrow range of migration rates, whereas extinction dominates the high as well as low migration rate regimes. Oscillatory dynamics are observed in the low and high m regime as well. However, these dynamics are much more sensitive to noise than the ones observed at intermediate migration rates. In

particular, the same bifurcation diagram generated from simulations with 2% noise in migration rate and dilution factor (inset in **A**) shows that complex oscillatory dynamics at intermediate m are preserved over 100 daily dilutions whereas those at low as well as high m disappear. Axes in the inset are identical to those in (A). **B)** A representative simulation time series of the ratio of AmpR to ChlR cells at $m = 0.04$ showing complex deterministic oscillations that resemble noisy out of phase period-2 dynamics.

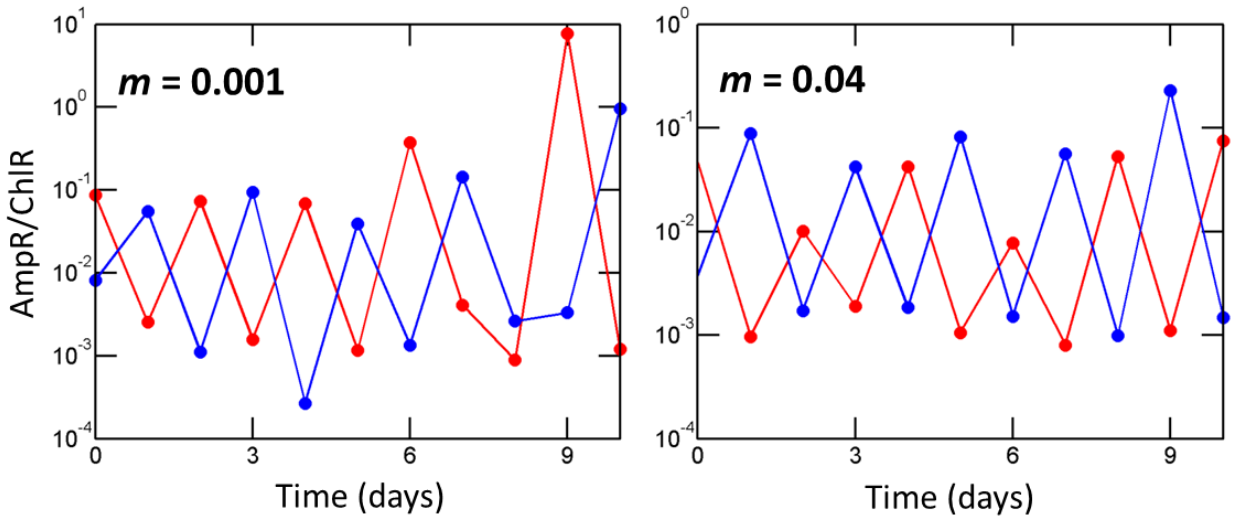

Fig. S5: Representative time series showing experimental evidence of out-of-phase period-2 oscillations in the harsh environment (10 μg/ml of ampicillin, 16 μg/ml of chloramphenicol) for $m = 0.001$ (left panel) and $m = 0.04$ (right panel). The period-2 oscillations at $m = 0.001$ appear to transform to a different period, illustrating that transient dynamics may also play an important role in governing survival in harsh environments.

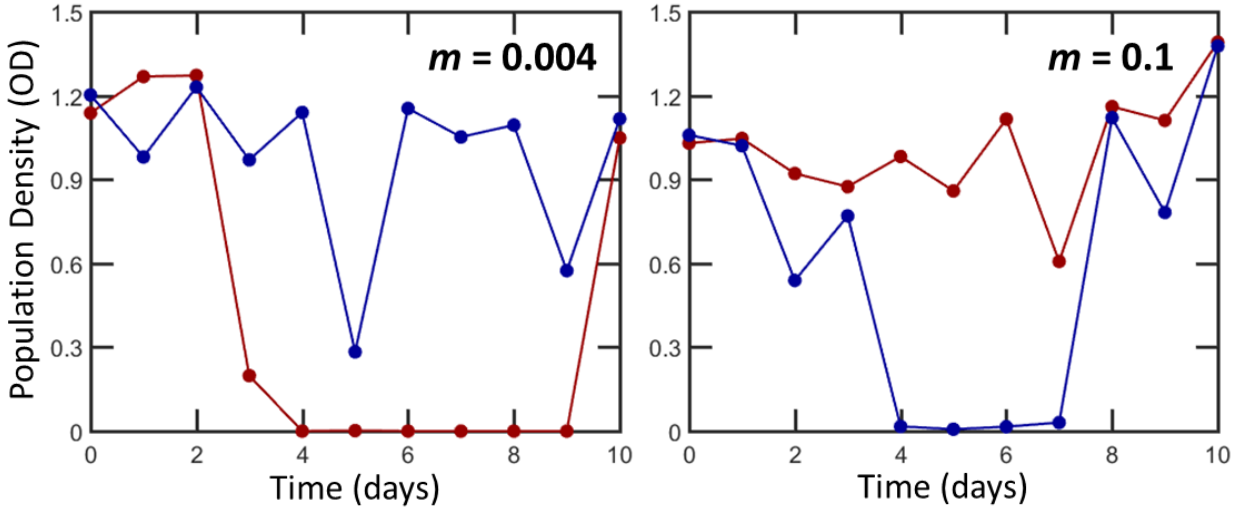

643

644 **Fig. S6:** Representative population density (OD) time series showing experimental evidence of
645 re-colonization events. We observe that one of the populations appears to go extinct, but recovers
646 a few days later due to migration from its partner.

647

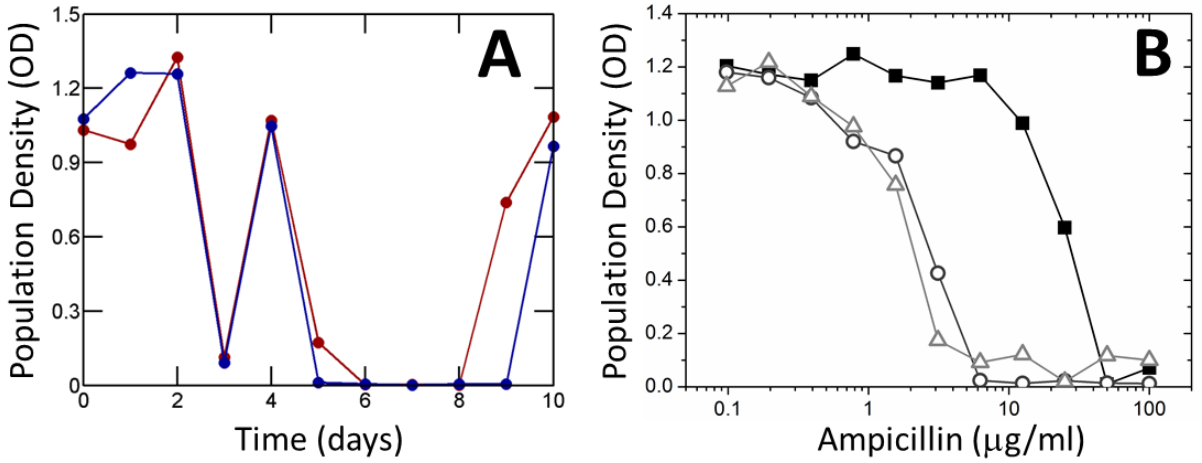

Fig. S7: Evidence for the chloramphenicol resistant strain (ChlR) evolving additional resistance to ampicillin in the harsh environment (10 μg/ml of ampicillin, 16 μg/ml of chloramphenicol). **A)** A representative population density (OD) time series ($m = 0.5$) in which both populations in a pair appear to go extinct, but one of them (red curve) rises again on day 9 and re-colonizes its partner, as seen from the rise in the blue curve on day 10. **B)** We measured the concentrations of ampicillin that inhibit growth of the ancestral ChlR strain before the migration experiment (open grey triangles), a biological replicate of the same ancestral ChlR strain after the experiment (open dark grey circles), and the evolved ChlR strain at the end of 9 days of the migration experiment (solid black squares). We observe that the evolved strain has tenfold higher resistance to ampicillin as compared to the ancestral strain.

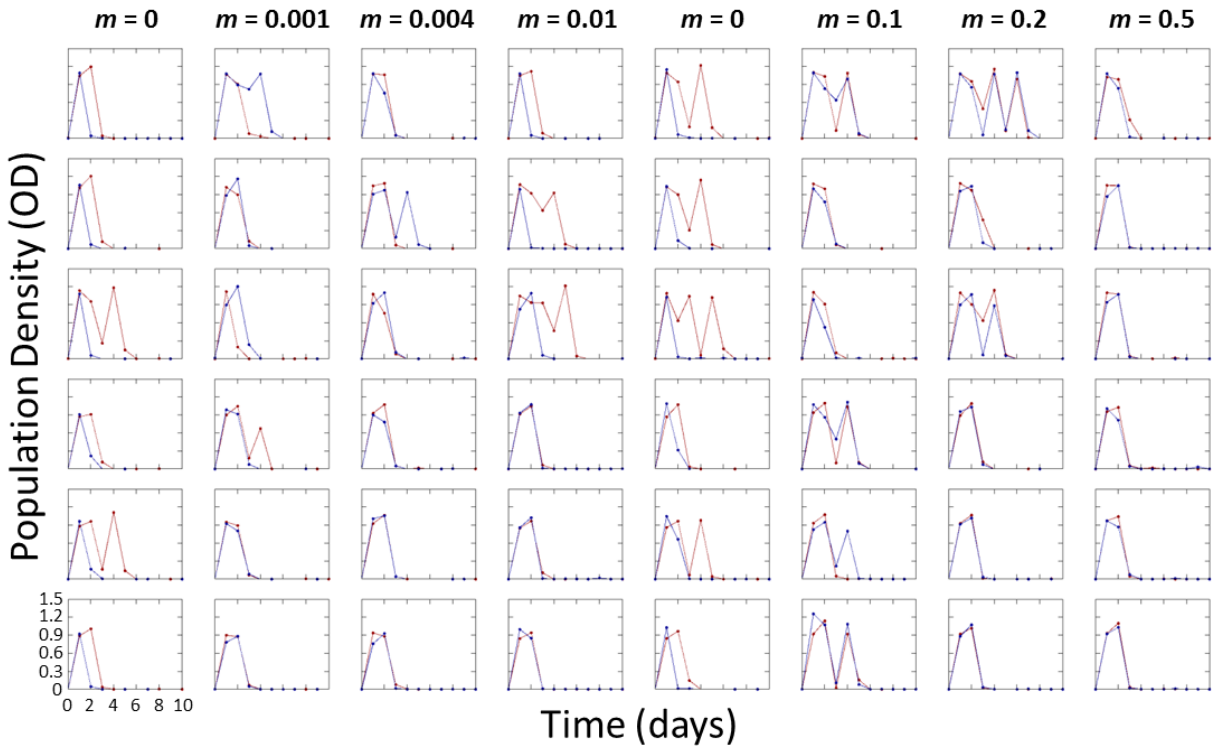

660

661 **Fig. S8:** Time series data for the population density (OD) in an extremely harsh environment (10
662 μg/ml of ampicillin, 20 μg/ml of chloramphenicol) for all 8 migration rates studied. All
663 populations become extinct within 7 days and there is no evidence for evolution of higher
664 antibiotic resistance.

665

Parameter	Meaning	Value used
γ_1^R	Growth rate of AmpR cells in the absence of chloramphenicol	1.18/hr
γ_2^R	Growth rate of ChlR cells in the absence of ampicillin	1.21/hr
γ_2^D	Death rate of ChlR cells at high ampicillin concentrations	0.25/hr
I_{12}	Inhibitory concentration for AmpR cells in chloramphenicol	0.65 μg/ml
I_{21}	Inhibitory concentration for ChlR cells in ampicillin	1.3 μg/ml
K_m	Michaelis-Menten constant for ampicillin inactivation	12 μg/ml
V_{max}	Maximal hydrolysis rate of ampicillin	20000 $\frac{\mu g}{ml.hr.K}$
c_2	Inactivation rate of chloramphenicol	12.8 / (hr.K)
t_{lag}	Lag time during which no growth occurs but antibiotics can be deactivated	1 hr
K	Carrying capacity (density)	1
N_{min}	Lowest viable population density (finiteness of population size)	1 cell ≡ 10^{-8}

Table S1: The table lists the values of parameters used in our simulations. The population density is measured in units of the carrying capacity. In experiments, the carrying capacity of ChlR and AmpR cells is ~2.3 x 10^6 cells/μl.